Switching plasticity in compensated ferrimagnetic multilayers for neuromorphic computing

Weihao Li(李伟浩), Xiukai Lan(兰修凯), Xionghua Liu(刘雄华), Enze Zhang(张恩泽), Yongcheng Deng(邓永城), and Kaiyou Wang(王开友)

Citation: Chin. Phys. B, 2022, 31 (**11**): 117106. DOI: 10.1088/1674-1056/ac89dd

What follows is a list of articles you may be interested in

Uniaxial stress effect on quasi-one-dimensional Kondo lattice $CeCo_2Ga_8$

Kangqiao Cheng(程康桥), Binjie Zhou(周斌杰), Cuixiang Wang(王翠香), Shuo Zou(邹烁), Yupeng Pan(潘宇鹏), Xiaobo He(何晓波), Jian Zhang(张健), Fangjun Lu(卢方君), Le Wang(王乐), Youguo Shi(石友国), and Yongkang Luo(罗永康)

Chin. Phys. B, 2022, 31 (**6**): 067104. DOI: 10.1088/1674-1056/ac6339

Influence of thickness on current-induced magnetization switching in $L1_0$-FePt single layer

Shi-Qi Zheng(郑诗琪), Kang-Kang Meng(孟康康), Zhen-Guo Fu(付振国), Ji-Kun Chen(陈吉堃), Jun Miao(苗君), Xiao-Guang Xu(徐晓光), and Yong Jiang(姜勇)

Chin. Phys. B, 2021, 30 (**10**): 107101. DOI: 10.1088/1674-1056/ac0a62

Recent progress on excitation and manipulation of spin-waves in spin Hall nano-oscillators

Liyuan Li(李丽媛), Lina Chen(陈丽娜), Ronghua Liu(刘荣华), and Youwei Du(都有为)

Chin. Phys. B, 2020, 29 (**11**): 117102. DOI: 10.1088/1674-1056/abaed5

Giant interface spin-orbit torque in NiFe/Pt bilayers

Shu-Fa Li(李树发), Tao Zhu(朱涛)

Chin. Phys. B, 2020, 29 (**8**): 087102. DOI: 10.1088/1674-1056/ab9292

A review of current research on spin currents and spin-orbit torques

Xiao-Yu Feng(冯晓玉), Qi-Han Zhang(张琪涵), Han-Wen Zhang(张瀚文), Yi Zhang(张祎), Rui Zhong(钟瑞), Bo-Wen Lu(卢博文), Jiang-Wei Cao(曹江伟), Xiao-Long Fan(范小龙)

Chin. Phys. B, 2019, 28 (**10**): 107105. DOI: 10.1088/1674-1056/ab425e

---

RAPID COMMUNICATION

Switching plasticity in compensated ferrimagnetic multilayers for neuromorphic computing

Weihao Li(李伟浩)[1,2], Xiukai Lan(兰修凯)[1,2], Xionghua Liu(刘雄华)[1,2], Enze Zhang(张恩泽)[1,2], Yongcheng Deng(邓永城)[1,2], and Kaiyou Wang(王开友)[1,2,3,4,†]

[1] *State Key Laboratory for Superlattices and Microstructures, Institute of Semiconductors, Chinese Academy of Sciences, Beijing* 100083, *China*
[2] *Center of Materials Science and Optoelectronics Engineering, University of Chinese Academy of Sciences, Beijing* 100049, *China*
[3] *Beijing Academy of Quantum Information Sciences, Beijing* 100193, *China*
[4] *Center for Excellence in Topological Quantum Computation, University of Chinese Academy of Sciences, Beijing* 100049, *China*

(Received 16 June 2022; revised manuscript received 21 July 2022; accepted manuscript online 16 August 2022)

Current-induced multilevel magnetization switching in ferrimagnetic spintronic devices is highly pursued for the application in neuromorphic computing. In this work, we demonstrate the switching plasticity in Co/Gd ferrimagnetic multilayers where the binary states magnetization switching induced by spin–orbit toque can be tuned into a multistate one as decreasing the domain nucleation barrier. Therefore, the switching plasticity can be tuned by the perpendicular magnetic anisotropy of the multilayers and the in-plane magnetic field. Moreover, we used the switching plasticity of Co/Gd multilayers for demonstrating spike timing-dependent plasticity and sigmoid-like activation behavior. This work gives useful guidance to design multilevel spintronic devices which could be applied in high-performance neuromorphic computing.

Keywords: switching plasticity, compensated ferrimagnet, spin–orbit torque, spike timing-dependent plasticity, sigmoidal neuron, handwritten digits recognition, neuromorphic computing

PACS: 71.20.Eh, 75.50.Gg, 84.35.+i, 85.70.–w **DOI:** 10.1088/1674-1056/ac89dd

1. Introduction

Neuromorphic computing inspired by biological brain is getting increased attention attributing to ultralow-power compared to the traditional computers.[1–3] The nonvolatile neurons and synapses can process data *in situ*, which avoids the unnecessary energy cost of the data movement between different modules.[4] Besides, neuromorphic computing not only aims to achieve significant energy saving but also attempts to improve the efficiency during performing complex tasks including cognition, control, movement, and decision making.[5,6] Although various artificial neural networks algorithms have been developed in recent years, the lack of dedicated hardware still limits the application of neuromorphic computing.[7] Recently, spintronic devices have exhibited great potential in neuromorphic computing,[8–19] since they can simulate the functions of neurons and synapses, such as nonlinearity,[9] stochasticity[8,20] and nonvolatility.[1,21] Moreover, the fast dynamics[22,23] and virtually unlimited endurance make them stand out from other competitors including phase-change,[24,25] floating gated[26] and resistive memory[6] devices.

Compensated ferrimagnets offer the combined advantages of both ferromagnets and antiferromagnets, namely, the rich methods of manipulation and/or detection of their magnetization, ultrafast and energy-efficient spin–orbit torque (SOT) switching.[22,27–29] These advantages make them promising candidates for neuromorphic computing devices. In spintronic-based neuromorphic computing, the multilevel spintronic devices based on domain-wall (DW) motion generated multi-resistance states have been used to emulate biological synapses.[30–32] However, the stochastic nature of the DW pinning and depinning relying on the defects may limit the performance of the devices. Thus, searching for well-controlled methods to allow a binary ferrimagnet to realize tunable current-induced multilevel magnetization switching behavior is one of the vital issues. Recently, the tunable multilevel SOT-induced magnetization switching by adjusting the magnitude of in-plane magnetic field or current pulse with a built-in in-plane magnetic field has been observed in a ferromagnet system which suggests the plasticity of switching behavior.[18,33] However, as far as we know, few works on the switching plasticity in ferrimagnets have been reported,[23] which is certainly an urgent topic to promote the application process for spintronic-based neuromorphic computing.

In this work, we perform experiments with perpendicular magnetic anisotropy (PMA) Co/Gd ferrimagnetic multilayers under various AlO_x thickness. Both the Co and Gd layers are atomically thin, and their moments are coupled antiferromagnetically to form an artificial compensated ferrimagnetic structure. We demonstrate the switching plasticity in the

†Corresponding author. E-mail: kywang@semi.ac.cn

Co/Gd compensated ferrimagnetic multilayers, that is, the binary switching characteristic can be tuned into a multi-state one as the domain nucleation plays a more dominating role during the magnetization switching. The magnitude of the domain nucleation barrier is dependent on the PMA of the multilayers and the external in-plane magnetic field. The excellent switching plasticity gives the ferrimagnets great potential for various neuromorphic computing applications. On the one hand, we demonstrate the spike timing-dependent plasticity (STDP) using the multilevel switching of the Co/Gd compensated ferrimagnetic multilayers. On the other hand, we demonstrate that a three-layers neural network using ferrimagnetic neurons can well recognize patterns in Modified National Institute of Standards and Technology (MNIST) database with accuracy more than 97%. Our work could provide useful information for designing future high-performance spintronic-based neuromorphic computing devices.

2. Method

The schematic stack structures, as shown in Fig. 1(a), Ta (1)/Pt (5)/[Co (0.36)/Gd (0.34)]$_6$/Pt (1)/AlO$_x$ (t) (thickness in nm) with $t = 0$, 0.5, 1, 1.5, and 2.0 were sputtered on Si/SiO$_2$ substrates by direct and alternating voltage sources at room temperature. The base pressure of the chamber was less than 1×10^{-8} Torr, and the argon pressure was set as 2 mTorr for AlO$_x$ and 0.8 mTorr for other targets during deposition. Subsequently, the samples were patterned into Hall bars devices with channel widths of 10 μm by standard photolithography and Ar-ion etching.

3. Results and discussion

Firstly, we measured the anomalous Hall effect resistance ($R_{\rm hall}$) under an out-of-plane magnetic field (H_z), as shown in Fig. 1(b). A small current of 0.1 mA was used to measure the magnetic state of the device. It is worth noting that all samples with different AlO$_x$ thicknesses (t) exhibit square-shaped magnetic hysteresis loop, indicating that the magnetization easy axis is along the z direction. The hysteresis loops show a positive $R_{\rm hall}$ polarity, which reflects that the magnetization in the films is Co-riched since the anomalous Hall effect resistance is dominated by Co in the Co–Gd system.[34] Notably, the magnetic hysteresis loops show a gradual switching behavior with increasing the thicknesses of the AlO$_x$ layer to 2 nm, indicating the switching plasticity in the Co/Gd multilayers.

Subsequently, the switching plasticity in the Co/Gd multilayers under various in-plane and PMA field was systematically investigated in Fig. 2. The pulsed current of width 10 ms was applied and then we measured the $R_{\rm hall}$ after each pulse at a low current of 0.1 mA. Figure 2(a) shows the magnetization switching driven by SOT under different in-plane fields (H_x) for the device with AlO$_x$ thickness of 1 nm. The squareness and switching ratio ($\Delta R_{\rm Ratio}$) of magnetization switching loops decrease with the increase of H_x, and the number of intermediate states increases. Here, $\Delta R_{\rm Ratio}$ is defined as the ratio of current-induced maximum change in Hall resistance to field-induced maximum change in Hall resistance. This phenomenon is also observed in other samples. Moreover, we set the magnitude of $H_x = 800$ Oe in all samples to check the impact of the AlO$_x$ thickness, as presented in Fig. 2(b).

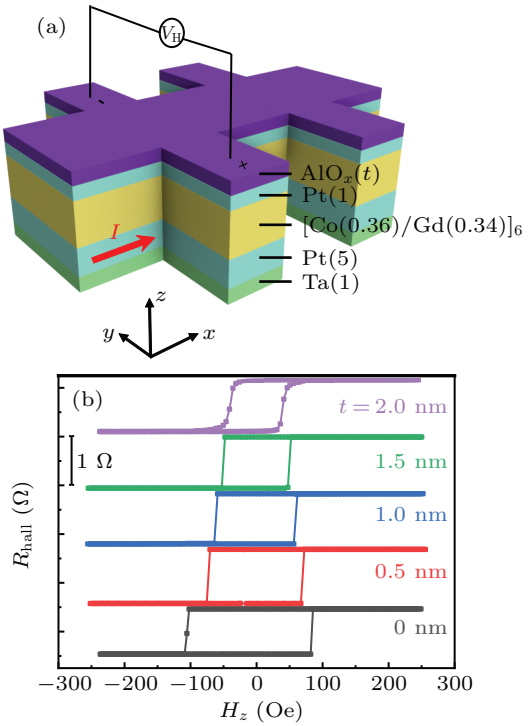

Fig. 1. (a) The schematic Hall device with stack structures of Ta (1)/Pt (5)/[Co (0.36)/Gd (0.34)]$_6$/Pt (1)/AlO$_x$ (t). (b) Anomalous Hall resistance $R_{\rm hall}$ as a function of perpendicular magnetic field H_z for various AlO$_x$ thickness.

Similarly, the samples with thicker AlO$_x$ are inclined to obtain multilevel magnetization switching behavior with a lower $\Delta R_{\rm Ratio}$ under the same in-plane field. The increasing AlO$_x$ thickness would reduce the effective PMA field of the device, which is because the strong interfacial 3d–5d hybridization in Co/Pt is weakened by the Pt/AlO$_x$ interdiffusion.[35,36] Then, we determine the effective PMA field ($H_{\rm k}$) of Ta(1)/Pt(5)/[Co(0.36)/Gd(0.34)]$_6$/Pt(1)/AlO$_x$(t) by fitting the in-plane field dependence of the in-phase first harmonic Hall voltage. In addition, the damping-like effective field of Ta(1)/Pt(5)/[Co/Gd]$_6$/Pt(1) is estimated by harmonic Hall voltage analysis, and the SOT efficiency is calculated to be 25 Oe/(1×10^7 A·cm^{-2}) (see the supporting information for details). The $H_{\rm k}$ as a function of the AlO$_x$ thickness is summarized in Fig. 2(f), which clearly shows the magnitude of $H_{\rm k}$ decreases with increasing the AlO$_x$ thickness. The magnetic moment of the samples with higher ratio of $|H_x|/H_{\rm k}$ would tilt away from the z direction corresponding to a larger angle (θ_M),

leading to a lower switching ratio in Figs. 2(a) and 2(b). Besides, a fatter switching curve is obtained accompanying with a lower $\Delta R_{\rm Ratio}$ (corresponding to a greater tilting angle θ_M). Thus, the relationship between the switching behavior and the tilting angle θ_M ($\propto |H_x|/H_{\rm k}$) needs to be further explored.

Then, we fixed the value of $H_x/H_{\rm k} \approx 0.5$ to check the impact of $H_{\rm k}$ on current-induced magnetization switching behavior, as presented in Fig. 2(c). The intermediate sates increase with increasing the thickness of AlO_x (corresponding to a lower $H_{\rm k}$). However, the switching ratio is roughly the same for all samples. Then we use ΔI to qualitatively evaluate the number of the intermediate magnetization states, which corresponds to the current range covering full $\Delta R_{\rm hall}$, as functions of H_x and AlO_x thickness. As clearly shown in Figs. 2(d)–2(f), ΔI increases nonlinearly with higher H_x and thicker AlO_x, which also indicates the switching behavior can be tuned by the in-plane magnetic field and/or effective anisotropy field. The broader current range accompanied by more multi-resistance states is useful for neuromorphic computing applications. Besides, the linearity of ΔI regulated by H_x and $H_{\rm k}$ is summarized in the supporting information.

In this section, we will go deep into the experimental phenomena and explain the switching plasticity which first shows sharp switching characteristic (binary state) then tunes to gradual switching one (multilevel) under increasing in-plane field. In general, magnetization switching takes place through DW propagation and domain nucleation.[37–39] It was verified experimentally that magnetic stripes with Néel-type chiral domain walls show sharp switching characteristics.[40] Compared to domain wall propagation, the nucleation switching induced by SOT is prone to provide gradual switching behavior, since they naturally form the basis of intermediate states.[17,33] The domain nucleation can be understood from an energy perspective. The probability of nucleation is proportional to $e^{-E_{\rm b}/k_{\rm B}T}$,[33] where $E_{\rm b}$, $k_{\rm B}$, and T are the nucleation energy barrier, Boltzmann constant, and the temperature, respectively. $E_{\rm b}$ has a spatial distribution across the sample which follows the normal distribution statistically. A higher $H_{\rm k}$ brings a higher energy barrier for domain nucleation while the in-plane field H_x can reduce the barrier.[33,41] Thus, the switching behavior depends on the magnitudes of $H_{\rm k}$ and H_x, as presented in Fig. 2. Moreover, the switching plasticity can also be explained by comparing the DW propagation field and nucleation field (see the supporting information for details).

After systematically studying the dependence of switching plasticity on the in-plane and PMA field, we then investigate how to use the plasticity of the magnetization switching for neuromorphic computing. Artificial neural networks (ANNs) and spiking neural networks (SNNs) are two important and complementary branches in neuromorphic computing with different advantages in dealing with practical tasks.[42] In the following section, the multi-level switching devices with excellent switching plasticity are exploited for both SNNs and ANNs.

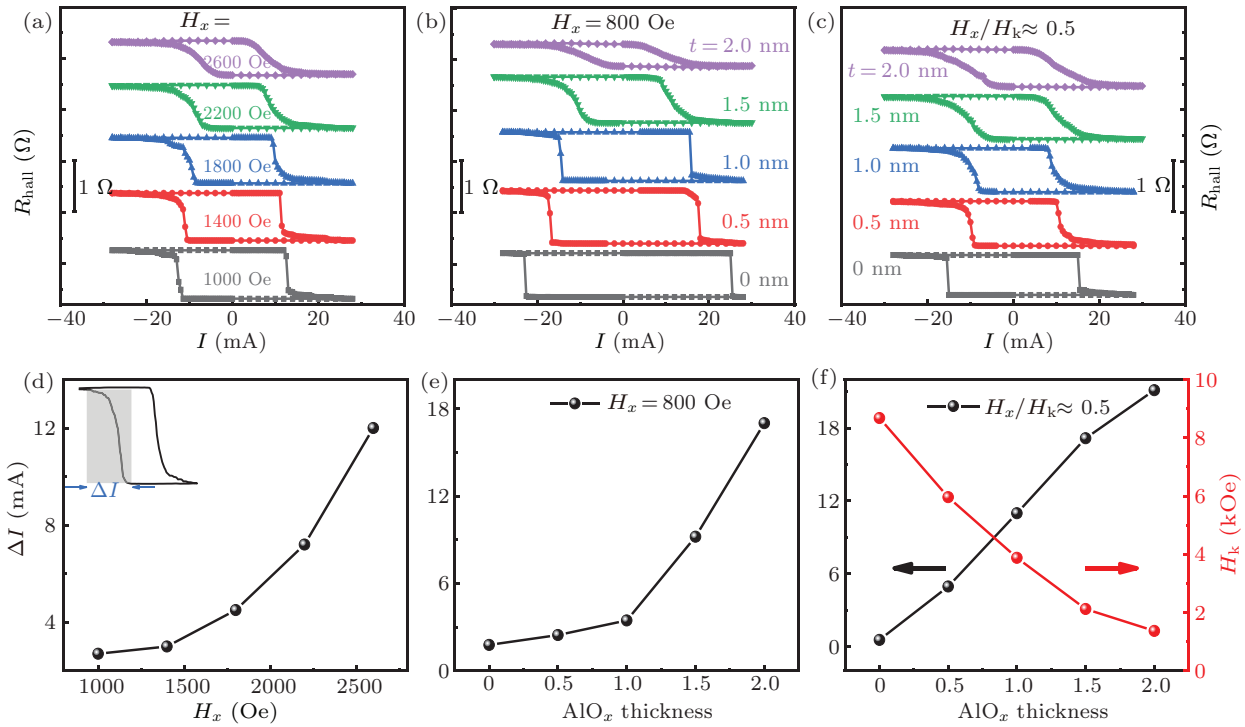

Fig. 2. (a) Pulsed current-driven $R_{\rm hall}$–I SOT switching loops under various H_x in Ta/Pt/[Co/Gd]$_6$/Pt/AlO_x (1). $R_{\rm hall}$–I SOT switching loops with different AlO_x thickness for H_x = 800 Oe (b) and $H_x/H_{\rm k} \approx 0.5$ (c) respectively. Tunable current range (ΔI) versus in-plane field H_x (d) and AlO_x thickness for H_x = 800 Oe (e). (f) AlO_x thickness dependence of the current range ΔI and PMA field $H_{\rm k}$ for $H_x/H_{\rm k} \approx 0.5$. The inset in (d) presents the current range ΔI we defined.

A synapse in SNNs builds the connection between the pre-neuron and post-neuron and its weights are updated when spikes and/or action potentials from the pre-neuron propagate to the post-neuron through the synapses. Moreover, the synaptic weight update rule depends on the delays between the spikes arriving from the pre- and post-neuron, which is known as STDP found in real biological synapses.[43] Figure 3(c) shows the dependence of the weight ($R_{\rm hall}$) with the amplitude of current pulses in our CoGd-based artificial synapse. The existence of well-defined current thresholds beyond which switching between low and high $R_{\rm hall}$ states occurs making it possible to implement STDP in our device. Based on the current pulse I dependence on the $R_{\rm hall}$, spikes as shown in Fig. 3(b) are designed for realizing the STDP in our device. Before the application of each single spike, a sequence of current pulses with decreasing amplitudes and alternating polarities was applied (e.g., $+28$ mA $\rightarrow -27.5$ mA $\rightarrow +27$ mA $\rightarrow \cdots \rightarrow -1.5$ mA $\rightarrow +1$ mA $\rightarrow -0.5$ mA) to achieve a zero $R_{\rm hall}$ state. When pre- and post-neuron spikes reach the CoGd multilayers with a delay Δt, their superposition produces the waveforms ($I_{\rm pre} - I_{\rm post}$) displayed in the inset of Fig. 3(d) (waveforms with various Δt could be found in the supporting information). We measure the change of $R_{\rm hall}$ produced by pairs of spike 1 and 2 with the time delay from -12 ms to 12 ms. Finally, the STDP window based on ferrimagnet artificial synapse is obtained where the weight ($|\Delta R_{\rm hall}|$) decreases with increasing $|\Delta t|$, as shown in Fig. 3(d). It obviously shows that the form of STDP can be tuned by the shape of spikes. We note that the symmetry of the STDP form is invariable under different H_x and $H_{\rm k}$ as shown in Fig. 2, hence the symmetry of the spike synapse is also retained. Notably, the performance of a certain learning procedure is highly dependent on the form of STDP in a spike neural network. Therefore, the form of STDP can be used to emulate various types of pre- and post-neuron activities.[44,45]

On the other hand, the nonlinear switching behavior of the ferrimagnetic multilayers makes it possible to construct a sigmoid neuron for an artificial neural network. Figure 4(a) shows the evolution of minor switching loops for Ta/Pt/[Co/Gd]$_6$/Pt/AlO$_x$(2) under $H_x = -500$ Oe by limiting the maximum pulsed current, and the presence of the minor loops indicates the intermediate magnetization states are non-volatility. Then we select one of the $R_{\rm hall}$–I curves (from -5 mA to 30 mA) in Fig. 4(a) to construct an artificial sigmoid neuron as an activation function for neural networks, as shown in Fig. 4(b). The input X is transformed to a current I applied into the devices, then $R_{\rm hall}$ is measured to represent the output Y. It is worth noting that a single SET pulse is required if a subsequent current pulse is higher than the previous one ($I > I_0$), however, an additional RESET pulse before the set pulse is needed to avoid the minor switching loops, as shown in Fig. 4(a). A modified sigmoid function is used to fit the experimental dates: $Y = 1/[1 + {\rm e}^{-(X-X_0)/K}]$, where K and X_0 represent the slope and the rising point of the function, respectively.

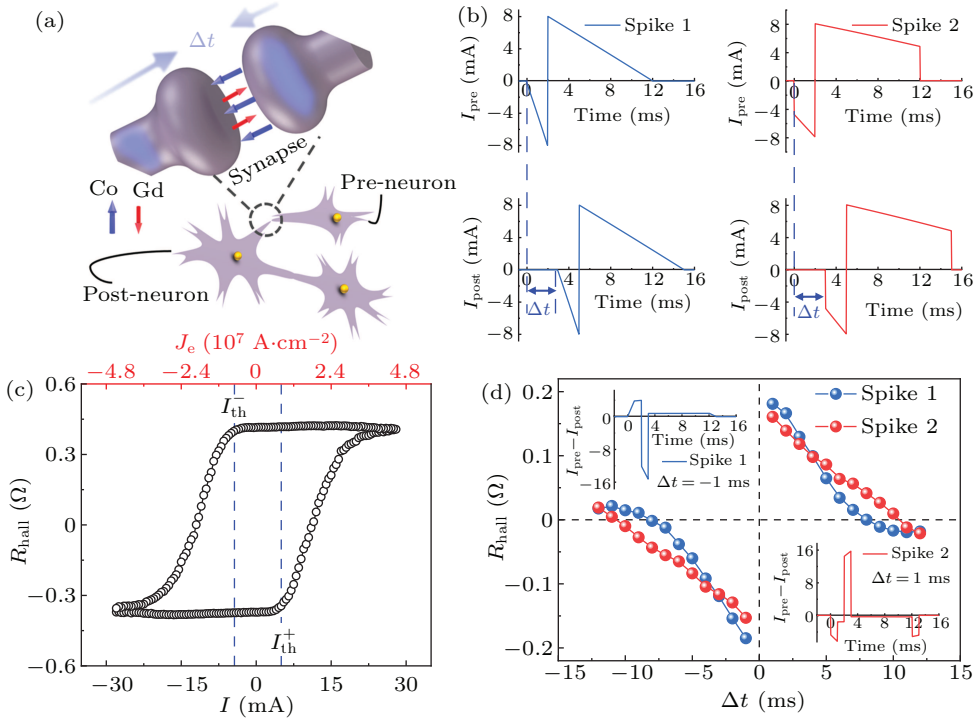

Fig. 3. (a) The illustration of CoGd-based artificial synapse. Spikes (blue) propagate between the neurons via synapses. (b) Two engineered spikes with different shapes named as spike 1 and spike 2, arriving from the pre-neuron and post-neuron. (c) Single-pulse $R_{\rm hall}$–I SOT switching loop displays clear current threshold ($I_{\rm th}$) for Ta/Pt/[Co/Gd]$_6$/Pt/AlO$_x$(2) under $H_x = -500$ Oe. (d) Measurement of STDP generated with spike 1 and spike 2. The device was demagnetized before each spike applied.

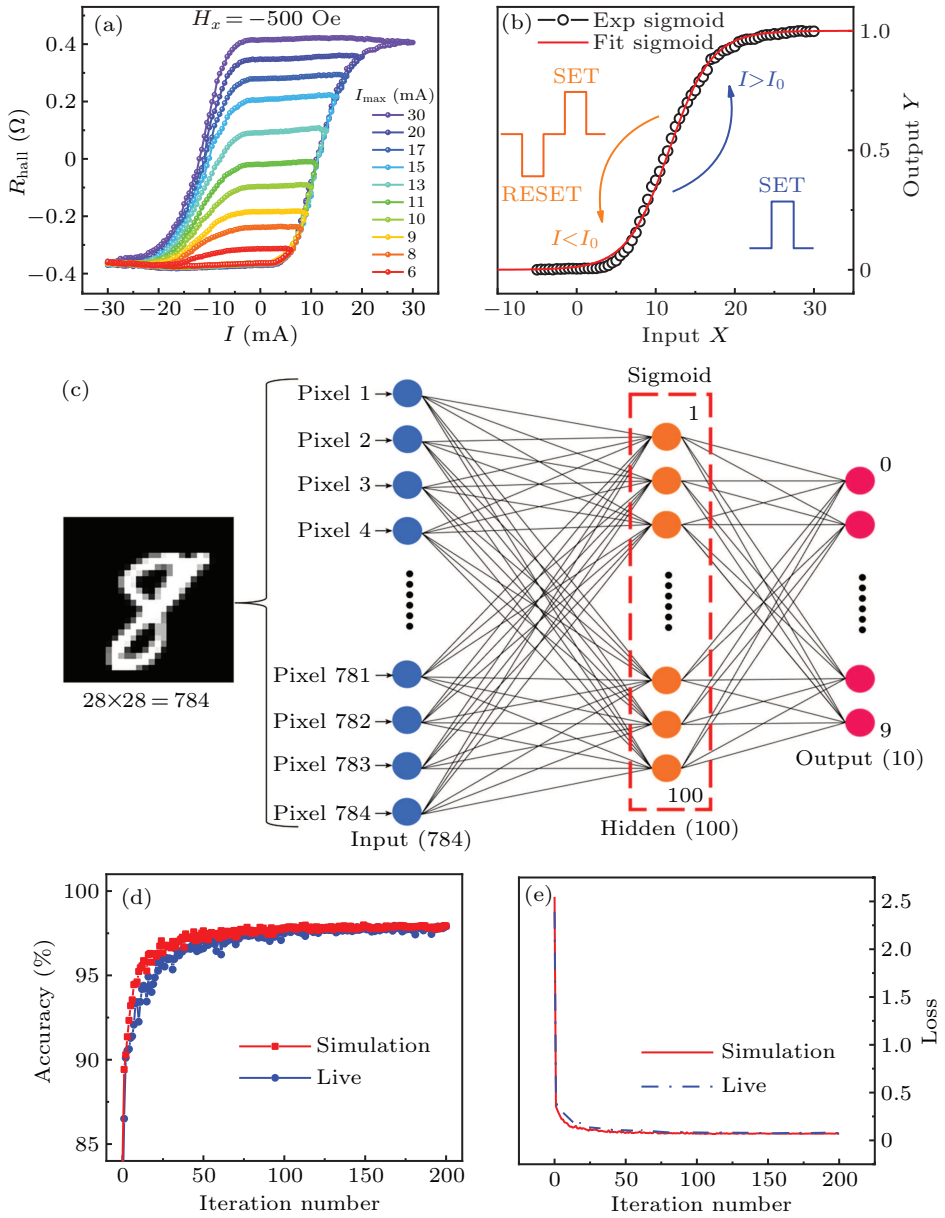

Fig. 4. (a) Minor switching loops (R_{hall} vs. I) with different maximum pulsed current (I_{max}) under $H_x = -500$ Oe. The current range is sweeping from −30 mA to I_{max}. (b) The normalized R_{hall} (output Y) as a function of pulsed current I (input X). (c) Three layers of neural network structure for handwritten digits recognition task. (d) Pattern recognition accuracy and (e) loss as a function of training iteration for an ideal sigmoid function (simulation) and experiment dates (live).

In order to evaluate the performance of the inference using the sigmoidal compensated ferrimagnetic neural, we construct a feed forward neural network based on gradient descent algorithm,[17,19] as presented in Fig. 4(c). It consists of three layers: an input layer of 784 neurons, a hidden layer of 100 neurons and an output layer of 10 neurons. Here, the MNIST handwritten pattern dataset consisting of labeled 60000 training examples and 10000 labeled testing samples is utilized as the written digit dataset. Figure 4(d) shows the recognition accuracy as a function of training iteration for experimental dates and ideal sigmoid function shown in Fig. 4(b). It is worth noting that our neural network based on Co/Gd multilayers neurons can achieve a high recognition accuracy of 97.7%, which is very close to the ideal software simulation (97.8%). The respective values of loss decrease quickly toward saturation, as shown in Fig. 4(e). Besides, the recognition accuracy is roughly independent of the in-plane field (see the supporting information for details). These training results prove the validity of our spintronic artificial sigmoidal neuron.

4. Conclusion

In summary, we have unambiguously tuned the switching behavior between binary state and multistate in Co/Gd multilayer. We find that the switching plasticity can be controlled by the nucleation energy barrier. Lowering the PMA and/or applying an in-plane field can lower the nucleation energy barrier, it thus can result in multilevel magnetization switching. We further used the switching plasticity for demonstrat-

ing neuromorphic computing. We demonstrate that the multilevel magnetization states in Co/Gd multilayer can not only act as a synapse to achieve spike timing-dependent plasticity, but also can as a neuron with sigmoid-like activation behavior. We have simulated an ANN to perform the pattern recognition tasks with an accuracy rate over 97%. Thus, the switching plasticity in compensated ferrimagnets not only provides useful guidance to design multistate spintronic devices, but also opens the prospective door for future high-performance neuromorphic computing.

Acknowledgements

This work was supported by Beijing Natural Science Foundation Key Program (Grant No. Z190007), Beijing Natural Science Foundation (Grant No. 2212048), the National Natural Science Foundation of China (Grant Nos. 11474272, 61774144, and 12004212), and the Chinese Academy of Sciences (Grant Nos. QYZDY-SSW-JSC020, XDB28000000, and XDB44000000).

References

[1] Chakraborty I, Jaiswal A, Saha A K, Gupta S K and Roy K 2020 *Appl. Phys. Rev.* **7** 021308
[2] Zidan M A, Strachan J P and Lu W D 2018 *Nat. Electron.* **1** 22
[3] Silver D, Huang A, Maddison C J, Guez A, Sifre L, van den Driessche G, Schrittwieser J, Antonoglou I, Panneershelvam V, Lanctot M, Dieleman S, Grewe D, Nham J, Kalchbrenner N, Sutskever I, Lillicrap T, Leach M, Kavukcuoglu K, Graepel T and Hassabis D 2016 *Nature* **529** 484
[4] Yang S, Kim K, Kim E, Baek K and Kim S 2009 *IEEE Trans. Consum. Electron.* **55** 2425
[5] Zhang Z, Wang S, Liu C, Xie R, Hu W and Zhou P 2022 *Nat. Nanotechnol.* **17** 27
[6] Wang Z, Joshi S, Savel'ev S, Song W, Midya R, Li Y, Rao M, Yan P, Asapu S, Zhuo Y, Jiang H, Lin P, Li C, Yoon J H, Upadhyay N K, Zhang J, Hu M, Strachan J P, Barnell M, Wu Q, Wu H, Williams R S, Xia Q and Yang J J 2018 *Nat. Electron.* **1** 137
[7] Maass W 1997 *Neural Netw.* **10** 1659
[8] Torrejon J, Riou M, Araujo F A, Tsunegi S, Khalsa G, Querlioz D, Bortolotti P, Cros V, Yakushiji K, Fukushima A, Kubota H, Yuasa S, Stiles M D and Grollier J 2017 *Nature* **547** 428
[9] Romera M, Talatchian P, Tsunegi S, Abreu Araujo F, Cros V, Bortolotti P, Trastoy J, Yakushiji K, Fukushima A, Kubota H, Yuasa S, Ernoult M, Vodeni-carevic D, Hirtzlin T, Locatelli N, Querlioz D and Grollier J 2018 *Nature* **563** 230
[10] Jung S, Lee H, Myung S, Kim H, Yoon S K, Kwon S W, Ju Y, Kim M, Yi W, Han S, Kwon B, Seo B, Lee K, Koh G H, Lee K, Song Y, Choi C, Ham D and Kim S J 2022 *Nature* **601** 211
[11] Grollier J, Querlioz D, Camsari K Y, Everschor-Sitte K, Fukami S and Stiles M D 2020 *Nat. Electron.* **3** 360
[12] Locatelli N, Cros V and Grollier J 2014 *Nat. Mater.* **13** 11
[13] Roy K, Jaiswal A and Panda P 2019 *Nature* **575** 607
[14] Song K M, Jeong J S, Pan B, Zhang X, Xia J, Cha S, Park T E, Kim K, Finizio S, Raabe J, Chang J, Zhou Y, Zhao W, Kang W, Ju H and Woo S 2020 *Nat. Electron.* **3** 148
[15] Kurenkov A, DuttaGupta S, Zhang C, Fukami S, Horio Y and Ohno H 2019 *Adv. Mater.* **31** 1900636
[16] Yang S, Shin J, Kim T, Moon K W, Kim J, Jang G, Hyeon D S, Yang J, Hwang C, Jeong Y and Hong J P 2021 *NPG Asia Mater.* **13** 11
[17] Zhou J, Zhao T, Shu X, Liu L, Lin W, Chen S, Shi S, Yan X, Liu X and Chen J 2021 *Adv. Mater.* **33** 2103672
[18] Cao Y, Rushforth A W, Sheng Y, Zheng H and Wang K 2019 *Adv. Funct. Mater.* **29** 1808104
[19] Lan X, Cao Y, Liu X, Xu K, Liu C, Zheng H and Wang K 2021 *Adv. Intell. Syst.* **3** 2000182
[20] Song M, Duan W, Zhang S, Chen Z and You L 2021 *Appl. Phys. Lett.* **118** 052401
[21] Fukami S, Zhang C, DuttaGupta S, Kurenkov A and Ohno H 2016 *Nat. Mater.* **15** 535
[22] Cai K, Zhu Z, Lee J M, Mishra R, Ren L, Pollard S D, He P, Liang G, Teo K L and Yang H 2020 *Nat. Electron.* **3** 37
[23] Liu J, Xu T, Feng H, Zhao L, Tang J, Fang L and Jiang W 2022 *Adv. Funct. Mater.* **32** 2107870
[24] Tuma T, Pantazi A, Le Gallo M, Sebastian A and Eleftheriou E 2016 *Nat. Nanotechnol.* **11** 693
[25] Suri M, Bichler O, Querlioz D, Cueto O, Perniola L, Sousa V, Vuillaume D, Gamrat C and DeSalvo B 2011 *2011 International Electron Devices Meeting (IEDM)* 4.4.1–4.4.4
[26] Ramakrishnan S, Hasler P E and Gordon C 2011 *IEEE Trans. Biomed. Circuits Syst.* **5** 244
[27] Kim S K, Beach G S D, Lee K J, Ono T, Rasing T and Yang H 2022 *Nat. Mater.* **21** 24
[28] Caretta L, Mann M, Büttner F, Ueda K, Pfau B, Günther C M, Hessing P, Churikova A, Klose C, Schneider M, Engel D, Marcus C, Bono D, Bagschik K, Eisebitt S and Beach G S D 2018 *Nat. Nanotechnol.* **13** 1154
[29] Siddiqui S A, Han J, Finley J T, Ross C A and Liu L 2018 *Phys. Rev. Lett.* **121** 057701
[30] Parkin S S P, Hayashi M and Thomas L 2008 *Science* **320** 190
[31] Leonard T, Liu S, Alamdar M, Cui C, Akinola O G, Xue L, Xiao T P, Friedman J S, Marinella M J, Bennett C H and Incorvia J A C 2022 *Adv. Electron. Mater.* 2200563
[32] Lequeux S, Sampaio J, Cros V, Yakushiji K, Fukushima A, Matsumoto R, Kubota H, Yuasa S and Grollier J 2016 *Sci. Rep.* **6** 1
[33] Wan C H, Stebliy M E, Wang X, Yu G Q, Han X F, Kolesnikov A G, Bazrov M A, Letushev M E, Ognev A V and Samardak A S 2021 *Appl. Phys. Lett.* **118** 032407
[34] Mimura Y, Imamura N and Kushiro Y 1976 *J. Appl. Phys.* **47** 3371
[35] Nakajima N, Koide T, Shidara T, Miyauchi H, Fukutani H, Fujimori A, Iio K, Katayama T, Nývlt M and Suzuki Y 1998 *Phys. Rev. Lett.* **81** 5229
[36] Zhu L, Ralph D C and Buhrman R A 2019 *Phys. Rev. Lett.* **122** 077201
[37] Aharoni A 1962 *Rev. Mod. Phys.* **34** 227
[38] Moritz J, Dieny B, Nozières J P, Pennec Y, Camarero J and Pizzini S 2005 *Phys. Rev. B* **71** 100402
[39] Kim S, Jang P H, Kim D H, Ishibashi M, Taniguchi T, Moriyama T, Kim K J, Lee K J and Ono T 2017 *Phys. Rev. B* **95** 220402
[40] Pai C F, Mann M, Tan A J and Beach G S D 2016 *Phys. Rev. B* **93** 144409
[41] Shibata J, Tatara G and Kohno H 2005 *Phys. Rev. Lett.* **94** 076601
[42] Pei J, Deng L, Song S, Zhao M, Zhang Y, Wu S, Wang G, Zou Z, Wu Z, He W, Chen F, Deng N, Wu S, Wang Y, Wu Y, Yang Z, Ma C, Li G, Han W, Li H, Wu H, Zhao R, Xie Y and Shi L 2019 *Nature* **572** 106
[43] Bi G and Poo M 1998 *J. Neurosci.* **18** 10464
[44] Zamarreño-Ramos C, Camuñas-Mesa L A, Pérez-Carrasco J A, Masquelier T, Serrano-Gotarredona T and Linares-Barranco B 2011 *Front. Neurosci.* **5** 26
[45] Boyn S, Grollier J, Lecerf G, Xu B, Locatelli N, Fusil S, Girod S, Carrétéro C, Garcia K, Xavier S, Tomas J, Bellaiche L, Bibes M, Barthélémy A, Saïghi S and Garcia V 2017 *Nat. Commun.* **8** 1